Use of Ultrafast Dispersed Pump−Dump−Probe and Pump−Repump−Probe Spectroscopies to Explore the Light-Induced Dynamics of Peridinin in Solution

Emmanouil Papagiannakis,*,† Mikas Vengris,†,§ Delmar S. Larsen,†,|| Ivo H. M. van Stokkum,† Roger G. Hiller,‡ and Rienk van Grondelle†

Department of Physics and Astronomy, Faculty of Sciences, Vrije Universiteit, De Boelelaan 1081, 1081 HV, Amsterdam, The Netherlands, and School of Biological Sciences, Macquarie University, NSW 2109, Australia

Received: June 9, 2005; In Final Form: November 14, 2005

Optical pump-induced dynamics of the highly asymmetric carotenoid peridinin in methanol was studied by dispersed pump−probe, pump−dump−probe, and pump−repump−probe transient absorption spectroscopy in the visible region. Dispersed pump−probe measurements show that the decay of the initially excited S_2 state populates two excited states, the S_1 and the intramolecular charge-transfer (ICT) state, at a ratio determined by the excitation wavelength. The ensuing spectral evolution occurs on the time scale of a few picoseconds and suggests the equilibration of these states. Dumping the stimulated emission of the ICT state with an additional 800-nm pulse after 400- and 530-nm excitation preferentially removes the ICT state contribution from the broad excited-state absorption, allowing for its spectral characterization. At the same time, an unrelaxed ground-state species, which has a subpicosecond lifetime, is populated. The application of the 800-nm pulse at early times, when the S_2 state is still populated, led to direct generation of the peridinin cation, observed for the first time in a transient absorption experiment. The excited and ground electronic states manifold of peridinin has been reconstructed using target analysis; this approach combined with the measured multipulse spectroscopic data allows us to estimate the spectra and time scales of the corresponding transient states.

Introduction

In contrast to higher plants, some photosynthetic marine organisms use mainly carotenoids rather than chlorophylls for the collection of light.[1] The dinoflagellate *Amphidinium carterae*, which is such an oceanic eukaryotic algae, uses the water-soluble peridinin chlorophyll protein (PCP) complex, as well as a peridinin-containing intrinsic light-harvesting complex (LHC), for capturing sunlight.[2] Many spectroscopic studies have attempted to characterize the properties of peridinin in solution,[3−12] and to relate them to the dynamics observed in PCP,[10,13−15] where peridinin transfers energy to chlorophyll-*a* (Chl-*a*) with high efficiency.[4,13]

Peridinin challenges the general consensus of using the idealized C_{2h} group symmetry to describe the excited-state properties of carotenoids.[16] As seen in Figure 1, peridinin has a structure unusual for carotenoids, with a C_{37} backbone and a π-electron conjugation length of ∼8 that extends on an allene moiety and a lactone ring. Furthermore, peridinin has rings at both ends of its conjugated chain. This structural complexity breaks the symmetry significantly and distinguishes peridinin from other carotenoids conferring its peculiar properties. Like for other carotenoids, its color is due to the strongly allowed transition from the ground-state S_0 to the S_2 state, which is short-lived and decays to the lower "dark" singlet electronic states.

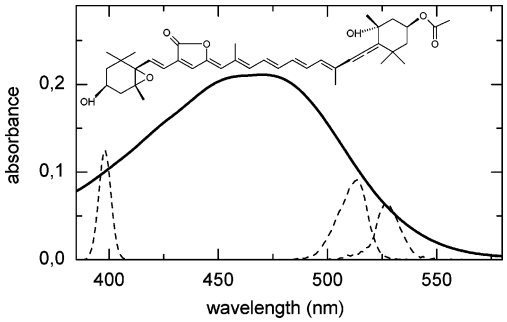

Figure 1. Chemical structure and steady-state absorption spectrum of peridinin in methanol. The dashed lines correspond to the spectra of the three different excitation pulses used in the experiments.

In most carotenoids, the properties of the S_1 state show no significant dependence on solvent polarity;[17] however, in peridinin, the spectral profile and the excited-state dynamics observed following the decay of S_2 show a pronounced dependence on the polarity and hydrogen-bonding properties of the environment.[5,7] These properties are interpreted in terms of a low-energy excited state with intramolecular charge transfer (ICT) character being populated together with S_1 during relaxation in polar solvents,[5] which moreover accounts for the near-IR stimulated emission (SE) band observed in methanol but not in hexane.[7] Studies which compared peridinin with other, structurally similar, carotenoids ascribed many of its special properties to the carbonyl group of the lactone ring.[6,18] These transient absorption studies suggested that the excited-state absorption (ESA) of peridinin in hexane, which peaks at ∼510 nm and has a low-amplitude tail to the red, corresponds to the "pure" S_1 state, with a 160-ps lifetime; in methanol, the ESA is

* To whom correspondence should be addressed. E-mail: papagian@nat.vu.nl. Fax: +31-20-5987999.
† Vrije Universiteit.
‡ Macquarie University.
§ Current Address: Vilnius University, Faculty of Physics, Quantum Electronics Department, Sauletekio 9-III, LT10222 Vilnius, Lithuania.
|| Current Address: Department of Chemistry, University of California, Davis, One Shields Avenue, Davis, CA 95616.

10.1021/jp053094d CCC: $33.50
Published on Web 12/14/2005

significantly broader with a peak at 590 nm and a lifetime of ~10 ps and corresponds to a mixture of S_1 and ICT.[5,7] Zigmantas et al.[8] conducted solvent−polarity, temperature, viscosity, and excitation−wavelength-dependence experiments and concluded that the S_1 and ICT states cannot be distinguished and that the ICT state is part of the potential energy surface of the S_1 state. Furthermore, the observed excited-state dynamics of peridinin in protic solvents depends on the excitation wavelength[8] and was ascribed to the presence of two structural forms which may result in an S_1 state with varying degrees of CT character.

Quantum chemical calculations have been used to describe the properties of the lower singlet excited states of peridinin, however different methods appear to give conflicting results. Shima et al[10] used MNDO-PSDCI theory and concluded that S_1 has a large dipole moment and *is* the ICT state and the large dipole was attributed to extensive mixing of the dark S_1 with the bright S_2 state. In contrast, time-dependent density functional theory calculations of Fleming and co-workers,[19] identify the ICT state as a separate electronic state whose energy is lowered in polar solvents, in agreement with the initial proposal of Frank and co-workers.[5]

Multiple channels are involved in the high efficiency of excitation energy transfer (EET) from peridinin to Chl-*a* in the PCP complex. Despite earlier claims from fluorescence upconversion,[4] transient absorption,[13] and theoretical calculations[20] that S_2 is not involved in energy transfer, it was shown that it is actively participating and donates ~30% of its energy to Chl-*a*.[14,15] The major channel of energy transfer in PCP is on the time scale of ~2.5 ps and involves the S_1/ICT states.[13−15] The participation of the peridinin ICT state in energy transfer in PCP was concluded from probing the SE band of the ICT state in PCP at 930 nm, whose decay matched the rise of the Chl-*a* bleach.[15] A faster, subpicosecond EET component was attributed to energy transfer to Chl-*a* from an unrelaxed excited state, probably a vibrationally hot ICT state. A contribution from similar carotenoid hot S_1 states has been found during EET in bacterial[21] and plant[22] LHCs. However, it is puzzling how the ICT state, whose emission maximum appears above 900 nm, can be an efficient energy donor to Chl-*a* which absorbs at 670 nm. Zigmantas et al. proposed that the spectral origin of the emission spectrum is high enough in energy to cover the Chl-*a* absorption;[15] alternatively, the emission may not reflect the energetic distance of the ICT state from the ground state because of a structural coordinate.[11] It may also be argued that if S_1 forms an efficient energy channel toward Chl-*a*, while in equilibrium with the ICT state, then the ICT state will reflect the Chl-*a* dynamics but may not need to be the direct donor. To address these important questions, the important relationship between the S_1 and ICT states must be first elucidated; to this end, we have applied different multipulse spectroscopic techniques.[23,24]

Multipulse Transient Absorption. The absorption−difference (ΔOD) spectra measured in pump−probe (PP) experiments are shaped by a number of qualitatively different contributions that may originate from different states of the system, for example, ground-state bleach, stimulated emission, and induced absorption (either by an excited state or by an unrelaxed ground state). One method of dissecting these contributions is by multipulse transient absorption methodologies, such as the dispersed pump−dump−probe (PDP) and the pump−repump−probe (PrPP) techniques, which involve the introduction of a third pulse to the PP experiment.[23,24] This additional pulse can be appropriately tuned and delayed to selectively interact with a "targeted" electronic transition. In PDP experiments, this added pulse interacts with the SE of an excited state and results in the de-excitation of molecules and the transfer of population from the excited state to the ground state. Consequently, it thereby decreases the ground-state bleach and the signals of the depleted excited state. In PrPP experiments, the additional pulse interacts with an ESA band and leads to the redistribution of the population within the excited-state manifold while the total amount of excitations is preserved, that is, the ground-state bleach is unaffected and only the signals of the repumped excited state change.

Ultrafast single-wavelength PDP experiments were previously used to study the elementary properties of the excited states in bacteriorhodopsin[25,26] and to explore ground-state dynamics in calmodulin;[27] asymptotic-limited dispersed PDP has been used to study ground-state liquid dynamics.[28] The higher excited-state dynamics of bacteriorhodopsin has been studied by single-wavelength PrPP,[29] and the combined use of PDP and PrPP allowed the distinction of overlapping bands in the PP signals.[25] We recently developed and applied multipulse spectroscopy with dispersed detection,[23,24] which allows the simultaneous probing of complete spectra, that subsequently can be analyzed globally.[30−32] This methodology was used on β-carotene dissolved in hexane to address the differences in the relaxation dynamics observed when excited by 400- or 500-nm laser pulses[24] and on peridinin in methanol, where it allowed the observation of the equilibration of the S_1 and ICT states after 530-nm excitation.[11]

Peridinin's complex excited-state structure makes it an ideal system to investigate with various multiple-pulse transient absorption techniques. It was previously shown that an 800-nm pulse can deplete the emissive ICT state by dumping its population to the ground state, which highlights excited-state properties;[11] the present work complements this study with a series of excitation wavelength-dependent PP, PDP, and PrPP measurements and provides a more complete picture of its potential energy surface. This paper is organized as follows: First, the results of PP experiments conducted with different excitation wavelengths are contrasted and analyzed with global analysis. Second, dispersed PDP and PrPP experiments with different excitation wavelengths are presented and are used to explore the potential energy surface of peridinin. Finally, target analysis of the PP and PDP data is used to characterize the excited and ground state of peridinin.

Materials and Methods

Sample Preparation. Peridinin was extracted from *Amphidinium carterae* thylakoids by the method of Martinson and Plumley[33] and was purified by reverse-phase HPLC using an Alltech C18 column. The samples were dried in vacuo and stored at −20° C; before the measurements, they were dissolved in methanol to a peak absorbance (475 nm) of ~0.3 in a 1-mm quartz cuvette. No sample degradation was observed during the experiment.

Ultrafast Transient Absorption. The PDP setup has been described in detail earlier.[23] The basis of the system is a 1-kHz amplified Ti:Sapphire system (Coherent-BMi α1000) delivering 450-μJ, 60-fs, 800-nm pulses. Part of the output of the amplifier was used to pump a homemade noncollinear optical parametric amplifier (NOPA) which was tuned to generate visible pulses. For the 800-nm PDP experiment, we used the pulses directly from the amplifier, while the 400-nm pump pulses were generated by doubling the amplifier output in a BBO crystal. A small part of the 800-nm light was used for generating a

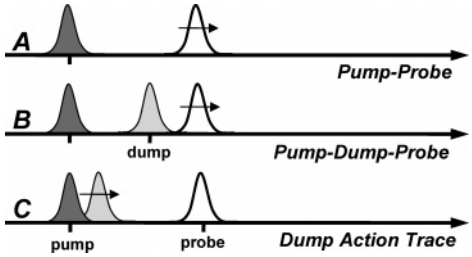

Figure 2. Three-pulse measuring schemes used in the experiments: (A) standard pump−probe, (B) pump−dump−probe kinetics, and (C) pump−dump−probe action trace. The horizontal axis denotes the time delay, and the arrows on pulses indicate their movement.

single-filament white-light continuum in a slowly translating CaF_2 crystal for broad-band probing. Separate computer-controlled optical translation stages allowed the precise timing of the three pulses. Reflective optics have been used to steer and focus the white-light probe beam to the sample, decreasing the group velocity dispersion to typically ~300 fs over the range of 400−700 nm. The pump and dump/repump pulses were maintained at the same polarization which was set at magic angle (54.7°) compared to that of the probe light. The time and wavelength resolutions of our experiments are 125 fs and 1 nm respectively, while the average noise level is <1 mOD.

Pulse Timing Schemes. Dispersed PDP and PrPP measurements generate multidimensional data (two time and one wavelength dimensions) which can be collected and presented in two different ways (Figure 2).[23,24] In a PDP kinetics measurement (Figure 2B), the dump pulse is placed at the selected "dump delay" after the pump pulse and remains fixed during the measurement. The dump delay corresponds to a specific distribution of excited-state population and thus determines the effect that will be induced. The probe pulse is delayed as in PP measurements and records the effect of the dump pulse on the spectrum and dynamics of the PP signal.

Alternatively, the dump-induced dynamics can be explored by measuring an "action trace" (Figure 2C),[23,24] in which the delay of the dump pulse is scanned while the probe pulse is maintained at a selected delay. An action trace monitors how the PP spectrum at the chosen probe delay changes as a consequence of the interaction of the dump pulse with the system at variable instances. An additional advantage of an action trace is that it is not affected by time-zero artifacts (e.g., cross-phase modulation, stimulated Raman scattering, two-photon absorption, etc.) because the probed signal is at a much longer delay, allowing clear observation of the dump-induced dynamic changes at early times.

Data Presentation and Analysis. Along with the ΔOD signals measured without (PP) and with (PDP) the dump pulse, we construct the double-difference signals

$$\Delta\Delta\mathrm{OD}(\lambda,t,\tau) = \mathrm{PDP}(\lambda,t,\tau) - \mathrm{PP}(\lambda,t) \qquad (1)$$

where λ and t represent the probe wavelength and delay and τ the delay of the dump pulse. The ΔΔOD signal is often easier to interpret as it has nonzero amplitude only when there is a dump-induced effect on the PP measurement. However, the time domain of the ΔΔOD signals inherently contains the dynamics of the underlying PP signal; to examine the occurrence of additional, purely dump-induced, dynamics we can construct the relative double-difference signal

$$\Delta\Delta\mathrm{OD}_{\mathrm{rel}}(\lambda,t,\tau) = \Delta\Delta\mathrm{OD}(\lambda,t,\tau)/\mathrm{PP}(\lambda,t) \qquad (2)$$

To fully characterize the experimental data, we used global and target analysis methodologies,[30−32] which allow the application of a specific physical model to describe the observed dynamics. For the description of the PP signals alone, we used a four-component sequential scheme to estimate the characteristic time scales for spectral evolution and decay and the corresponding evolution-associated difference spectra (EADS).[31,32] A sequential scheme consists of components that interconvert unidirectionally with increasing exponential lifetimes. The EADS estimated from such a scheme do not necessarily portray pure excited states but rather describe the spectral evolution. To estimate the species-associated difference spectra (SADS) that portray the *real* states of the system, the PDP data were analyzed simultaneously with the PP data by applying a specific physical model in target analysis.[31,32] In this description of the data, a connectivity scheme is chosen with each of its compartments depicting a distinct state of the system. The model applied in target analysis is designed to make physical sense, to produce plausible spectra, and to fit the data well.

Results

Excitation Wavelength-Dependent Pump−Probe Measurements. The excitation of peridinin in methanol at different parts of the S_2 potential surface results in different relaxation dynamics;[8] to fully characterize these dynamics, we collected dispersed pump−probe data with excitation at 400, 510, and 530 nm (Figure 1). The absorption changes were probed over the visible region to simultaneously monitor the dynamics of the ground-state bleach and the ESA of the S_1/ICT states. PP data with two different excitation wavelengths were collected concurrently; two excitation beams (400 *and* 510 nm or 400 *and* 530 nm) are directed onto the sample and are alternated by asynchronous chopping every ~6 ms; in this way, identical experimental conditions are maintained.[24]

Figures 3 and 4 summarize the measured pump−probe data. Figure 3 contains the PP spectra measured 1 ps (panel A) and 10 ps (panel B) after excitation at 400, 510, and 530 nm. In agreement with earlier observations,[8] the PP spectra measured 1 ps after excitation differ significantly, especially in the 500−550 nm region, where the ESA increases appreciably with bluer excitation. The ΔOD spectra measured at a delay of 10 ps (Figure 3B), with the three different excitation wavelengths, have similar shapes, which indicates that significant spectral evolution has occurred. Such spectral evolution might originate from solvation, vibrational relaxation, equilibration, charge stabilization, structural rearrangement, or a combination thereof.

Characteristic kinetic traces measured in the bleach (485 nm) and the ESA (535, 590 nm) regions are compared in Figure 4, illustrating the different dynamics related to the spectral evolution observed in the ΔOD spectra (Figure 3). To emphasize the differences in the dynamics, the traces have been normalized at 10 ps (indicated by arrows in the figure), when they correspond to time-resolved spectra of similar shape (Figure 3). At a probe wavelength of 590 nm, which predominantly reflects the ESA of the ICT state,[7] the 530-nm excitation produces a significantly larger signal than the 400 nm, while the signal after 510-nm excitation lies between. The convergence of all three traces to the same amplitude at 10 ps highlights the different decay dynamics; the trace measured after 530-nm excitation decreases significantly during the first few picoseconds, whereas the amplitude of the 400-nm excitation trace is essentially constant.

We applied a sequential scheme (1st EADS → 2nd EADS → 3rd EADS, etc.) in the global analysis to estimate the constituent EADS and lifetimes of the S_1/ICT states in the 400-

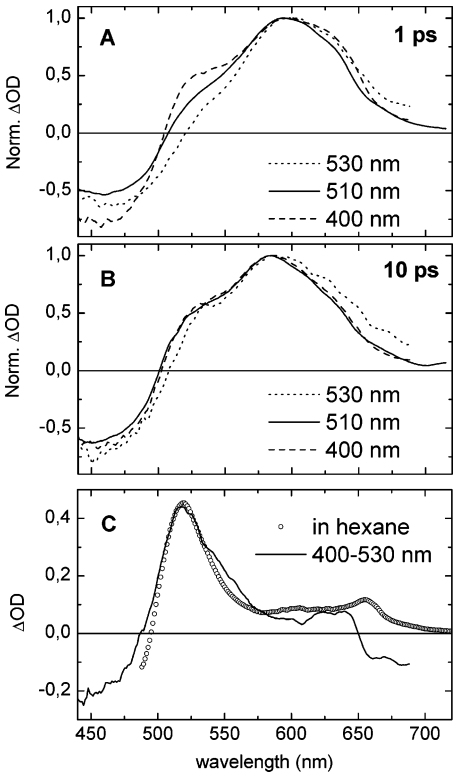

Figure 3. Pump−probe spectra measured after exciting peridinin in methanol at 400, 510, and 530 nm, normalized at their peak amplitude to emphasize their different shapes: (A) 1 ps after excitation and (B) 10 ps after excitation. (C) The difference between the spectra measured on peridinin in methanol after 400- and 530-nm excitation at a 1-ps delay, overlaid with the pump−probe spectrum of peridinin in hexane measured at 3 ps.

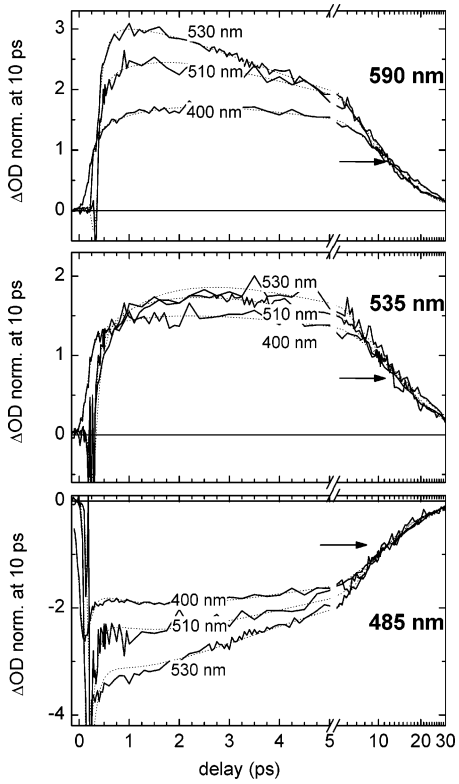

Figure 4. Pump−probe kinetic traces measured at 485, 535, and 590 nm (bleach, S_1/ICT ESA), after exciting peridinin at 400, 510, and 530 nm. The traces in each panel have been scaled to have equal amplitude ($\Delta OD = 1$) at a delay of 10 ps, which highlights their different dynamics. The dotted lines correspond to the global fit of the data with a sequential model (also see Figure 5).

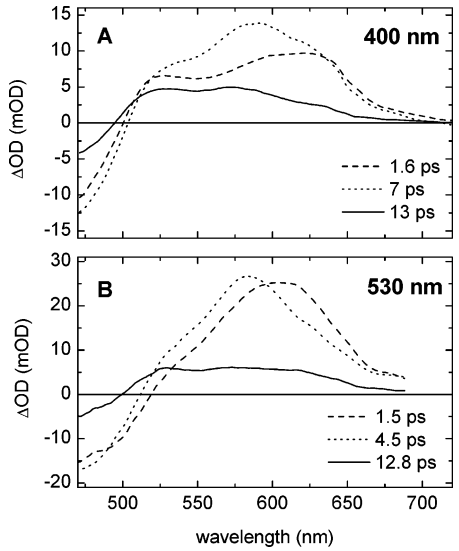

Figure 5. EADS and lifetimes corresponding to the S_1/ICT states of peridinin in methanol as estimated by the global analysis of the pump−probe data collected after 400- and 530-nm excitation, using a sequential model (also see Figure 4).

and 530-nm excitation PP measurements (Figure 5). Four exponential decays are required for a proper description of the data in both cases; the instantaneous EADS, depicting the S_2 state with an instrument-response limited time scale, has been omitted due to interfering artifacts around time zero. The second EADS (dashed lines), which has a 1.5 ps lifetime in the 530-nm and 1.6 ps in the 400-nm experiment, contains an intense ESA. This ESA exhibits a clear peak around 600 nm after 530-nm excitation, whereas after 400 nm it is much broader with a significant shoulder to the blue of 550 nm. In both experiments, the evolution to the third EADS (dashed to dotted lines) is characterized by a blue shift of ESA. After 530-nm excitation, the ESA peak shifts to 590 nm and the spectrum becomes narrower. A 590-nm peak becomes clear also after 400-nm excitation, but the spectrum remains broad both on the blue ($<$550 nm) and the red side ($>$620 nm). The third EADS evolves in 4.5 ps (530-nm excitation) and 7 ps (400 nm) to the fourth EADS (dotted to solid lines), which has similar shape and lifetime, ∼13 ps, in the two experiments. The relative amplitudes and the lifetimes of these three components are comparable to the single-probe wavelength results reported previously.[8]

An examination of the ESA blue shoulder helps to dissect the different contributions to the EADS. In methanol, the broad ESA above 550 nm is directly attributed to the ICT state,[5,7] whereas the shoulder on its blue side is ascribed to the "normal" S_1 state,[5,7] which is easily observed in hexane.[8] The PP spectra measured on peridinin in methanol after excitation at 400 and 530 nm (Figure 3A) differ significantly in the blue part of the ESA, suggesting that the contribution of the S_1 state depends on the excitation wavelength. A comparison of the PP spectrum measured in hexane, which depicts S_1, with the difference spectrum constructed by subtracting the 1-ps PP spectra measured with 400- and 530-nm excitation (Figure 3C), shows that the difference spectrum is markedly similar to that of S_1; thus, it may well originate from a variation in the amount of S_1 which is produced directly from S_2 after exciting peridinin in methanol at 400 or 530 nm. Furthermore, 1 ps after the excitation of peridinin at 400 nm the bleach signal below 500 nm increases (Figure 5A, dashed to dotted line), which can only

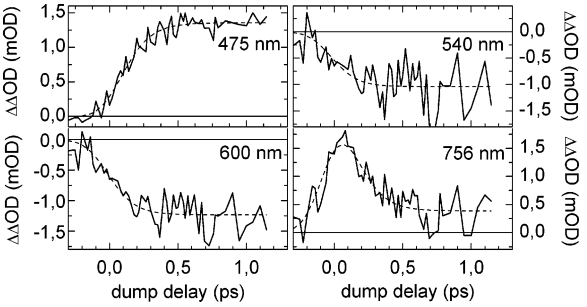

Figure 6. Action trace kinetics (ΔΔOD) measured at different probe wavelengths after 400-nm excitation. These traces are measured by varying the delay of the 800-nm pulse while the probe delay is fixed at 10 ps (with respect to the pump). The dashed lines indicate the global fit of the data with two exponentials.

be attributed to the decrease, on this time scale, of an ESA band which overlaps with the bleach. We can already postulate that this ESA decrease corresponds to a loss of S_1 population, which has ESA in this spectral region.[8] When peridinin is excited at 530 nm, the spectral evolution in this region is different; the blue ESA shoulder is weak at early delays, indicating that very little S_1 is populated. However, a few picoseconds later, the ESA in this region increases relative to the 590-nm band, indicative of an enhanced contribution from S_1. This spectral evolution, which takes place in both experiments on the time scale of a few picoseconds, can be attributed to the equilibration of the S_1 and ICT states.[11]

Three-Pulse Experiments: PrPP and PDP. Action Trace Dynamics. In an action trace measurement (Figure 2), the timing of the "additional" 800-nm pulse is changed while probing the asymptotic effect on a PP spectrum at a specific delay. Characteristic action trace kinetics measured at 475, 540, 590, and 756 nm after 400-nm excitation at a probe time of 10 ps are shown in Figure 6. The presence of two distinct time scales in the data is evident and is confirmed by a global fit that requires two exponential components, one of ~100 fs and one long-lived (dashed lines in Figure 6); the effect of the 800-nm pulse on the 10-ps PP spectrum changes significantly over time. In the ESA region (540 and 600 nm), the change of the PP signal (i.e., the ΔΔOD signal) is negative, due to a loss of ESA signal within a picosecond. Concomitantly, the ΔΔOD signal in the bleach region (475 nm), where the PP signal is negative, is positive indicating a partial recovery of the bleach, that is, a loss of excited-state population. We can safely conclude that this process corresponds to the dumping of the excited-state population to the ground state. An entirely different effect is observed at 756 nm, where the PP spectrum has almost no amplitude (Figure 3). A positive signal is present during the first ~200 fs, manifesting an interaction of the 800-nm pulse with the short-lived S_2 state. This signal describes a gain of ESA and cannot be attributed to any of the excited states of peridinin observed in the PP experiments above, suggesting the opening of a pathway that creates a new species. In the following sections, we will address separately these two different effects.

Repumping of Excited Peridinins. The S_2 state of peridinin has a strong ESA in the near-IR,[8] so when the 800-nm pulse is applied at early delays it can re-excite the S_2 population into a higher excited state (i.e., a PrPP process). In principle, the relaxation from this higher state should return the population to S_2 and subsequently to the S_1/ICT states on a subpicosecond time scale, without affecting the 10-ps PP spectrum. It is therefore striking that, upon repumping the S_2 state, a gain of ESA signal is observed above 700 nm where ESA of the S_1/ICT states is small. This increase of absorption on the 10-ps

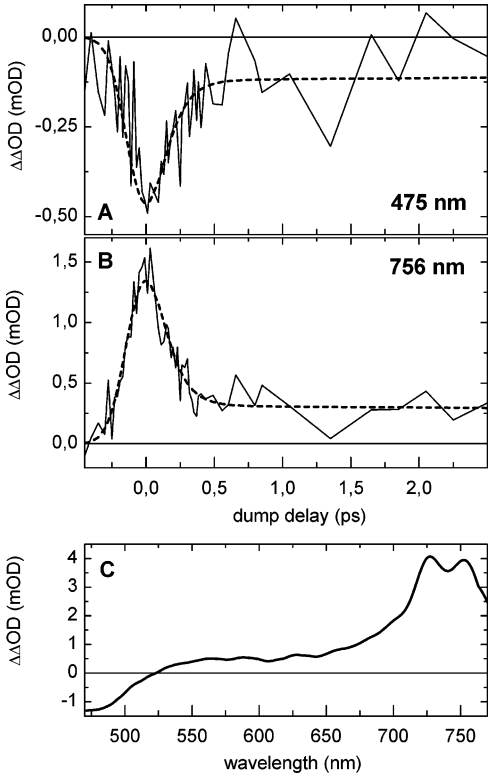

Figure 7. (A, B) Action trace kinetics (ΔΔOD) measured at the bleach (475 nm) and on the red edge (756 nm) of the visible spectrum, after 400-nm excitation and 800-nm repumping of the S_2 state. The delay of the 800-nm pulse is varied while the probe delay is fixed at 50 ps. The dotted lines denote the fit. (C) The fitted spectrum of the excited species that is generated by the interaction of the S_2 state with the 800-nm pulse. The induced absorption peak at ~750 nm indicates that it corresponds to a peridinin cation.

PP spectrum shows that the 800-nm repump does not redistribute the excited population within the known excited states but instead populates a new species.

To study the properties of this species and to obtain its spectrum, we measured a PrPP action trace with the probe delay set at 50 ps, when the S_1 and ICT states have decayed. In this experiment, the newly found species is temporally isolated and its full spectrum can be measured free from other interfering signals. The resulting action trace signals (Figure 7A and B) show that this process also involves a bleach signal, indicating that it corresponds to an excited peridinin. To fit the data globally, we needed two exponential components, of which the first, with a 110-fs lifetime, had significant amplitude, confirming that the generated species originates mostly from S_2. The spectrum of this species, which was also estimated by the global fit (Figure 7C), exhibits a bleach below 520 nm and absorption further to red, rather weak and featureless below 670 nm, but with a peak around 670−770 nm. The presence of an additional long-lived component (Figure 7A and B), which has an identical spectrum but negligible amplitude (<15%), implies that a longer-lived state can also generate this species. This may occur via the repumping of a weak ESA, such as that of the S_1 state, which overlaps with the SE band of the ICT state.[8] The dynamics of this new excited species was examined by placing the 800-nm pulse at ~100 fs, to maximize its yield, and measuring its kinetics. No decay was observed within 4 ns (data not shown) indicating that it is not a singlet excited state of peridinin but, as argued in the discussion section, the peridinin cation. To further investigate its occurrence, we carried out PrPP experiments on the S_1/ICT states. Visible pulses, of 550 and

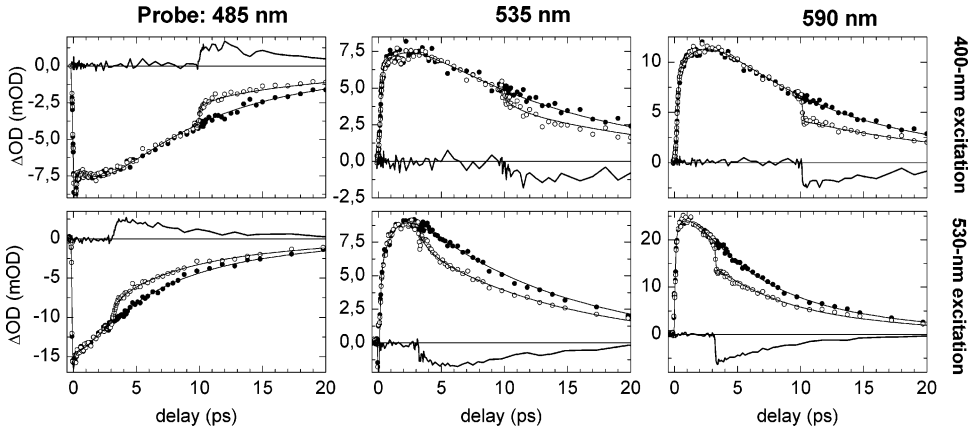

Figure 8. Pump−dump−probe kinetics: pump−probe signals are shown by filled circles, pump−dump−probe signals by open circles, and ΔΔOD signals by solid lines. Upper row: data measured with 400-nm excitation and dumping by 800 nm at 10 ps. Bottom row: data measured with 530-nm excitation and dumping by 800 nm at 3 ps. The lines through the data points correspond to the target analysis fit.

620 nm, were used to repump the intense S_1/ICT ESA, and in both cases, we observed an instantaneous loss of signal followed by a full recovery (Supporting Information Figure S1). No gain of absorption above 700 nm or long-lived signal were observed, implying that the recycling of the excited-state population through the normal $S_2 \rightarrow S_1$/ICT relaxation channel was complete.

800-nm Pump−Dump−Probe. PDP spectroscopy is a powerful tool in separating coexisting excited-state signals and identifying their origins. The spectral and temporal dynamics that evolve after a 800-nm dump pulse was applied when peridinin was excited at 530 nm were instrumental in characterizing the relationship between the S_1 and ICT states.[11] In this section, we will compare the PDP signals measured after exciting peridinin at 400 and 530 nm and by dumping, with 800 nm, at different times to explore the dumping effects at different phases of the relaxation.

When peridinin was excited at 400 nm and the ICT state was dumped after 10 ps (Figure 8, top row), all three probe wavelengths exhibited an amplitude loss. The decrease of bleach signifies the ground-state population recovery and confirms the dumping. In the second PDP experiment (530-nm excitation with the 800-nm dump at 3 ps, Figure 8, lower row), the results are rather similar and the ESA decreases upon interaction of the 800-nm pulse with the excited peridinins, while the ground state shows a recovery.

To highlight the spectral aspects of the depletion, we normalize and contrast the ΔΔOD spectra measured 0.5 and 11 ps after the dump with the corresponding PP spectra (Figure 9). The ΔΔOD spectrum measured 0.5 ps after dumping (thick solid lines in Figure 9A,C) is narrow in both experiments and is distinctly different from the PP spectrum (thin solid lines), as it does not contain the blue shoulder. This spectrally incomplete loss of the blue part of the ESA implies that the 800-nm dump pulses preferentially reduce the ICT population more than the S_1 population. Contrasting the ΔΔOD spectra measured 0.5 and 11 ps after the dump pulse (Figure 9) shows that further spectral evolution takes place, which is similar in both the 400- and 530-nm excitation experiments. The ΔΔOD spectra measured 11 ps after the dump (thick solid lines in Figure 9B and D) have significant amplitude in the 520−550 nm region and are identical to the corresponding PP spectra (thin solid lines). Although the instant depletion of the ESA is only partial (Figure 9A and C), the final loss is homogeneous across the ESA band (Figure 9B and D) and all excited states (ICT *and* S_1) contributing to the ESA suffer a population loss after a few picoseconds after the dump pulse (see also Supporting Information, Figure S2).

The dynamics initiated by the dump process in the ESA region are more evident in the $\Delta\Delta OD_{rel}$ signal (eq 2, Figure 10**).** This signal isolates the *pure* dump-induced dynamics, unlike the ΔΔOD signal which contains both the PP and PDP dynamics in the time domain. The traces measured at 535 nm and 590 nm preferentially probe the "S_1" and the "ICT" ESA contributions; different time scales are distinctly observed in these $\Delta\Delta OD_{rel}$ signals and confirmed by a global fit of the $\Delta\Delta OD_{rel}$ data, which requires three exponential components (dotted lines in Figure 10). In both PDP experiments (400- and 530-nm excitation), the ICT signal (590 nm probe) diminishes instantly (instrument-response limited) upon dumping, whereas the depletion of the S_1 population (535-nm probe) is on a time scale of picoseconds. In the bleach region (475-nm probe), the dynamics corresponds to the recovery of the ground-state population after the dump; however, in both experiments, the ground-state recovery does not follow the instantaneous loss of ICT but instead exhibits a finite, subpicosecond response. The presence of three distinct time scales (instantaneous, subpicosecond, and picosecond) illustrates that, as shown already earlier for the 530-nm excitation,[11] also after 400-nm excitation the dump populates an unrelaxed ground-state intermediate (GSI) species, which subsequently relaxes to the ground state.

The spectral overlap of ESA and bleach in the region around 500 nm, where both the S_1 and the GSI contribute, makes the assignment to specific processes complicated. Hence, the application of target analysis (see below), to analyze the complete PP and PDP measurements, is mandatory for the characterization of the temporal and spectral dynamics and the attribution to specific processes.

Target Analysis: Excited-State Connectivity. The PP and PDP experiments described above establish that the S_1 and ICT states of peridinin are separate, yet coupled, entities, which equilibrate on a picosecond time scale. Both states are produced with excitation-wavelength-dependent yields; excitation with 400-nm pulses produces significant S_1 population, while red-wing excitation with 530-nm pulses creates almost exclusively the ICT state. These findings have been confirmed by the PDP experiments, as dumping the SE of the ICT state induced only a partial loss of ESA, which became uniform after a few picoseconds as a result of the S_1/ICT equilibration. Additionally, the dumping of a significant ICT population allowed the

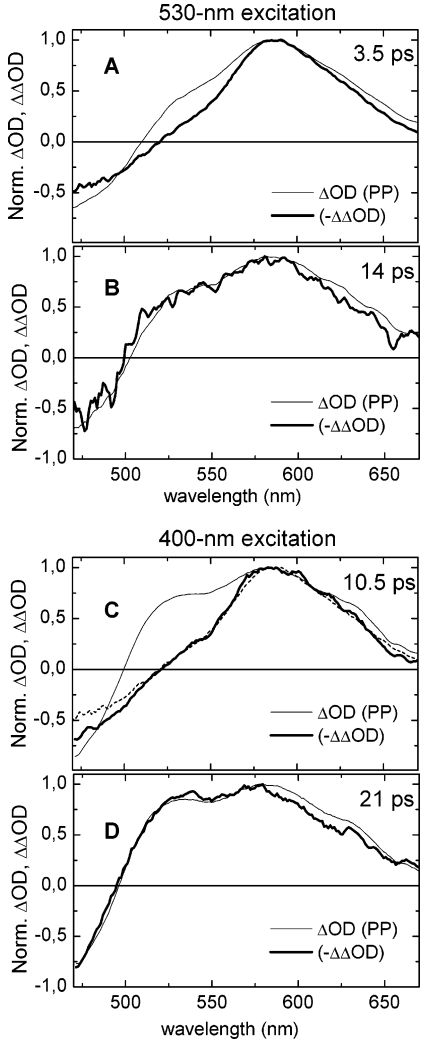

Figure 9. Comparison between the pump−probe spectra (thin lines) and the (inverted for convenience) ΔΔOD spectra (thick lines). 530-nm excitation: probed (A) 0.5 ps and (B) 11 ps after dumping of the ICT state by 800-nm pulses (3 ps after excitation). 400-nm excitation: probed (C) 0.5 ps and (D) 11 ps after dumping of the ICT state by 800-nm pulses (10 ps after excitation). The 0.5-ps ΔΔOD spectrum of panel A (the thick line) is also included in panel C (as a thin dotted line) to allow the comparison between the 0.5-ps ΔΔOD spectra measured in the two experiments. All spectra have been normalized at the peak of the excited-state absorption.

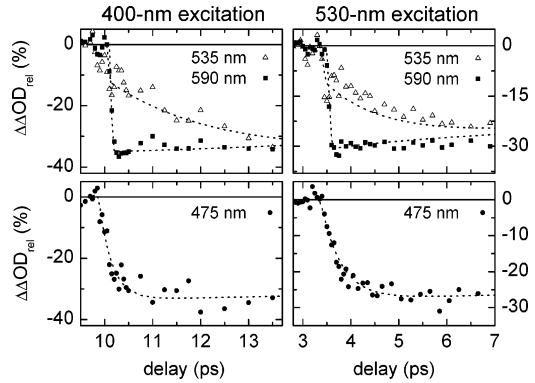

Figure 10. Relative loss of PP signal, $\Delta\Delta OD_{rel}$, which is induced by the 800-nm dump pulse, after 400- and 530-nm excitation, measured at different wavelengths. The dotted lines indicate the global fit of the data with three exponentials.

observation of an unrelaxed ground-state species, which relaxes to the ground state with a subpicosecond lifetime. We have

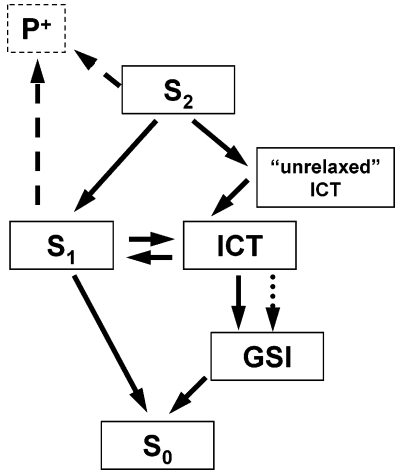

Figure 11. Excited-state model that we have applied in fitting *simultaneously* the pump−probe and pump−dump−probe data measured with 400- and 530-nm excitation and 800-nm dumping of the ICT state. The solid arrows represent the natural relaxation processes and the dotted arrow the dump mechanism. The dashed arrows denote the repump processes that produce the peridinin cation which have not been considered in the modeling.

modeled the PP and PDP results by using target analysis methodologies[30−32] to disentangle the dynamics of these states and to estimate their SADS.

The connectivity scheme (Figure 11) that was earlier applied to describe the data collected with 530-nm excitation[11] has now been used to also describe the 400-nm excitation data. Five compartments were essential for the simultaneous fit of the PP and PDP data. Relaxation from the initially excited S_2 state is modeled to occur via two separate pathways, the first populating the S_1 state and the second the ICT state. Only the latter involves an unrelaxed intermediate, which may involve solvation, vibrational relaxation, or structural reorientation dynamics. Even though the S_1 state is also likely to be undergoing subpicosecond thermal relaxation, observed as a blue shift of ESA in other carotenoids,[34−36] it has not been possible to resolve it here, probably because its red wing (where the relaxation effect would be prominent) overlaps with the strong ESA of the ICT state. Furthermore, in the 530-nm excitation experiment, the S_1 is not produced from S_2 but via the ICT state, and thus, in this experiment, the higher vibrational levels of S_1 may never get populated. In our analysis, the lifetime of the S_1 state has been fixed to 160 ps, the value measured in hexane,[5,7] because the decay of "normal" carotenoid S_1 states has been shown to be solvent independent.[6] The populations of the S_1 and ICT states are allowed to equilibrate, and the decay of the ICT state (either naturally or via the applied dump pulse) populates an unrelaxed GSI state, which in turn decays to the ground state.

The target analysis involves fitting the PP and the PDP data simultaneously to the same scheme so that the model describes *both* experiments consistently. Additional information contained in the PDP experiment is used to extract the spectral and temporal information (branching ratios, equilibration time constant, "pure" SADS, ground-state relaxation) that cannot be estimated on the basis of the PP data alone. Time scales and relative yields were varied until the results of the fit fulfilled the following criteria: (A) The S_1 SADS should resemble the PP spectrum measured in hexane, where it is presumed to be the dominantly populated excited state (Figure 3C). (B) The ICT SADS, having no S_1 contributions, should contain little of the blue shoulder. (C) The unrelaxed ground state should decay to the ground state within a picosecond, corresponding to the

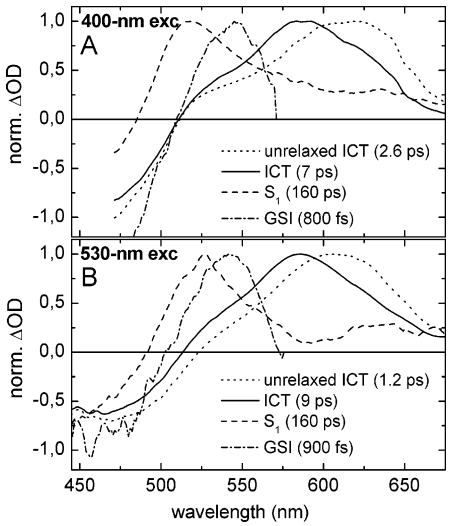

Figure 12. SADS of the S_1, ICT, and GSI states of peridinin in methanol that have been estimated by the simultaneous target analysis of the pump−probe and pump−dump−probe experiments (see also Figure 8). The SADS have been normalized at their maximum: (A) pump at 400 nm, dump by 800 nm at 10 ps; (B) pump at 530 nm, dump by 800 nm at 3 ps.

recovery of the bleach signal (Figure 10). Furthermore, we applied the spectral constraint that the SADS of the GSI has zero amplitude above 575 nm, assuming that the GSI spectrum must be similar to that of the ground state but slightly red shifted.

The estimated SADS and their lifetimes are shown (normalized) in Figure 12. The S_2 SADS is unreliable due to time-zero artifacts and is therefore not shown, but the separation of the other states has been successful as the SADS fulfill the criteria outlined above. The only discrepancy is in the SADS corresponding to the unrelaxed ICT intermediate; after 530-nm excitation, this component is devoid of S_1 features, whereas in the case of the 400-nm excitation it contains some ESA in the 500−550-nm region, suggesting that its separation from S_1-like components is not fully successful. Moreover, it has a 2.6 ps lifetime which is rather unrealistic when compared with the value estimated by the global analysis of the PP data alone with a sequential model.

The spectrally selective dump of the ESA has enabled us to estimate the SADS of the ICT state, which is similar for the two experiments. The lifetime of the ICT state is estimated to be 9 ps (7 ps) after 530-nm (400-nm) excitation. The SADS of the S_1 state peaks around 520 nm and has a tail to the red, resembling the one measured when peridinin is dissolved in hexane. The SADS that describes the GSI is similar in both experiments; it contains the ground-state bleach up to 510 nm and an absorption band peaking at 545 nm and decays to the ground state with a lifetime of 900 fs (800 fs).

The equilibration between the S_1 and ICT states occurs within 4.5 ps (7 ps after 400-nm excitation), a time scale which results from the combined dynamics of $S_1 \rightarrow$ ICT, ICT $\rightarrow S_1$, and ICT $\rightarrow$ GSI. The slow internal conversion $S_1 \rightarrow S_0$ ensures that most of the S_1 population shifts via the equilibration to the ICT state which then decays to the GSI. Within the specific model, the decay rates that are estimated by the target analysis fit have an uncertainty of ±5%. We found that similarly good fits to the data could also be obtained with the use of slightly different connectivity models; however, only the model in Figure 11 fulfilled all the criteria set above and produced reasonable SADS for all the measured data (400- *and* 530-nm excitation, PP *and* PDP) and was thus adopted. Finally, the decay rates estimated for the two experiments differ, however their qualitative picture as described by the model is essentially the same.

Discussion

Earlier transient absorption studies on peridinin demonstrated the relation between the polarity of the solvent and the decay lifetime and spectral shape of the ESA.[5,7] It was first suggested by Frank and co-workers that a low-lying ICT state exists, whose energy is stabilized in a polar environment distinct from S_1.[5] The shortening of the excited-state lifetime in polar solvents was attributed to the decay via the ICT state.[5,6] Recent calculations[10] suggest that the ICT does not exist as a separate state, but it *is* the S_1 state which has a strong dipole moment. Zigmantas et al. initially hypothesized an inversion of lifetimes, that is, a slow S_1-ICT relaxation followed by rapid ICT-S_0 decay[7] but later concluded that the ICT is a perturbation on the S_1 potential which is stabilized in polar environments.[8] In contrast, Fleming and co-workers,[19] who used time-dependent density functional theory to calculate the excited states of peridinin, found clear evidence of a distinct ICT state, separated from S_1.

Earlier we showed that in peridinin there is an excited-state equilibrium between the S_1 and ICT states.[11] Here, we present more complete results, with excitation wavelength-dependent PP and PDP measurements, to corroborate this claim. The PP data show that the decay following the excitation of peridinin to the S_2 state is multiexponential and is characterized by significant spectral evolution. The spectral shapes and decay amplitudes that we obtain after exciting peridinin in methanol at 400, 510, and 530 nm vary significantly (Figures 3 and 4). The most striking difference is observed immediately after excitation as the relative magnitude of the S_1 part of the ESA decreases dramatically as the excitation shifts to the red, whereas the PP spectra measured at later delays (Figure 3B) have comparable shapes. An excitation wavelength dependence of the decay dynamics has also been observed in other carotenoids.[24,37,38] However, the effect there is not as dramatic as in peridinin because these carotenoids do not feature a lactone ring.

In peridinin, three components were needed in the global analysis to describe the evolution and decay of the S_1/ICT states (Figure 5). A fast, ∼1.5 ps component is present in all three PP measurements and accounts for a blue shift of the ESA. Zigmantas et al. ascribed a similar rise component which they observed at 950 nm[8] purely to an increase of SE from the ICT state due to its structural stabilization. However, the spectral evolution corresponding to this process indicates that it may also contain dynamics such as the vibrational cooling observed in several other carotenoids[34−36] and solvation, which are expected to occur on a similar time scale.[39] In agreement with these results,[8] we observe that 530-nm excitation leads to a significant 4.5-ps component describing a significant loss of ESA (Figures 3 and 4). Furthermore, this intermediate component is also present, albeit smaller, after exciting at 510 nm (6.5 ps) and 400 nm (7 ps); in the case of 400-nm excitation, it mainly describes a loss in the red part of the ESA. This component carries the significant spectral evolution which leads to the final SADS, which has a similar shape in all experiments, indicating that it corresponds to the final, equilibrated mixture of the S_1 and ICT states.

Excited-State Equilibration. A large loss of the ESA signal is observed upon dumping the ICT state with 800-nm pulses (Figure 8) and is followed by resolvable dump-induced dynamics. Part of the loss is instantaneous and corresponds to a

decrease of the ICT-state ESA and the complicated evolution that follows can be separated into two distinct processes: (1) the formation and decay of a ground-state intermediate which was shown by the slow response of the bleach and (2) the excited-state relaxation of S_1 population toward the ICT state.

Target analysis has successfully disentangled these states and has allowed the clarification of the processes behind their complex spectral and temporal dynamics. The $S_1 \rightarrow S_0$ decay rate is much slower than the $S_1 \rightarrow$ ICT rate, and additionally, the ICT state has a short lifetime. The PP data indicate that after excitation of peridinin in methanol at 400 nm, the S_1 state receives population directly from the S_2 state, whereas after excitation at 530 nm, the S_1 is populated primarily after the equilibration with the ICT state. In both cases, the S_1 population decays via the equilibration with that of the ICT state which decays to the ground state via the GSI.

Ground-State Evolution. The GSI can only be observed after the dumping of ICT-state population; in PP experiments it never accumulates population because its lifetime is much shorter that that of the preceding ICT state. The absorption of the GSI appears upon the dumping on the blue side of the ESA of the ICT state and is depleted only when the GSI fully relaxes. The response of the bleach signal to the dump allows the estimation of the GSI lifetime, which is 900 and 800 fs after 530- and 400-nm excitation, respectively. Since the GSI is seen after dumping the ICT state at both an early stage (530-nm excitation, 3 ps) and a late stage (400-nm excitation, 10 ps), we may assume that the relaxation of peridinin always occurs via a GSI.

The nature of the GSI state is uncertain; such a species may arise from a vibrationally hot ground state, structural deformation, solvent dynamics, or some combination thereof. The subpicosecond vibration relaxation in the S_1 state of carotenoids has been observed in PP experiments,[34−36] however, the ground-state vibrational relaxation dynamics has not been established;[24] time-resolved resonance Raman measurements suggest that it takes several picoseconds.[40,41] GSIs similar to the one observed here were observed in PDP experiments on isomerizing chromophores in solution and were ascribed to "twisted" ground-state conformers with the resulting subpicosecond relaxations occurring along structural coordinates.[23,42] Additionally, the GSI lifetime is comparable to the time scales found for the excited-state solvation dynamics of coumarin in methanol.[39] Since the ICT state is strongly coupled to the polar environment, the nascent ground-state population generated by the applied dump pulse should undergo ground-state solvation, which has been shown to occur on similar time scales as the excited-state analogue.[27] Separating and identifying these effects is not trivial. The ICT state is stabilized in polar solvents, suggesting that its formation is precipitated by the generation of a macroscopic polarization by the high dielectric constant environment, which in turn may stabilize small scale structural changes in peridinin as suggested earlier.[8] We postulate that the GSI demonstrates a complex relaxation coordinate which reflects both ground-state solvation dynamics and structural changes. Since this GSI is observed both at the early stages of the ICT formation (3 ps dump) and at the later stages (10 ps dump), it supports the recent observation that a structural change occurs while in the S_2 state and that the ICT state potential energy surface is far from the Franck−Condon region of the excitation.[12]

Revealing the relationship of the S_1/ICT states and the presence of the GSI allow us to discuss the energy-transfer mechanisms in PCP, where peridinin transfers energy to Chl-*a* with a high efficiency,[4,13] from the S_2 and the S_1/ICT states.[14,15] The SE band of the ICT state was also observed in PCP with its decay time matching the rise of the Chl-*a* bleach at 670 nm, suggesting that the ICT state is an important energy donor.[15] However, the SE of the ICT state appears in the near-IR, whereas the Q_y state of Chl-*a* absorbs at 670 nm, $\sim$4000 cm^{-1} higher. The discovery of a complicated potential energy surface on the ground state demonstrates that the wavelength of the emission of the ICT state is not necessarily a measure for its absolute energy as it does not denote a transition to the relaxed ground state. This may account for the energetic difference between the peridinin ICT state and the Q_y level of Chl-*a*.

Peridinin Cation Generation. Previous PrPP experiments in β-carotene[24,43] showed a persistent loss of excited-state population after repumping the tail of the S_1 ESA at 800 nm. No product state was observed, and the repumped population disappeared, most probably deposited in a long-living state with no clear spectral signature in the probed region. On the contrary, when the S_1 of β-carotene state was repumped with a 550-nm pulse, 50% of the affected population was recovered after cascading through the higher states.[24] In peridinin, when an 800-nm pulse was applied soon after excitation, part of S_2 population was transferred to a higher excited state. In contrast to β-carotene,[24,43] a clear repumped photoproduct state is observed for peridinin, which does not decay on a nanosecond time scale and so is not a singlet excited state. The D_0-D_2 transition of carotenoid radicals is detected in the near-IR region, and moreover, the characteristic absorption of the cation of an eight double bond analogue of β-carotene in methanol has been reported at 760 nm.[44]

We thus ascribe the absorption band that we observe at 750 nm to the cation of peridinin, which is generated by the combined energy of the 400-nm excitation and the 800-nm repump pulses ($\sim$37 500 cm^{-1}), which is enough for overcoming the ionization threshold from S_2. Similarly, a small amount of radicals is also generated from the S_1 state as a result of repumping it with 800 nm, a combination that corresponds to a total energy of 28 600 cm^{-1}, if we use an S_1 energy of 16 100 cm^{-1}.[7] In sharp contrast, when a visible pulse was used to repump the intense ESA of the S_1/ICT state, no such species was observed, even though the total amount of energy exceeded $\sim$34 000 cm^{-1}. This illustrates that more factors than just the total energy of the molecule play a role in the generation of the radicals. This difference can be accounted for if we assume that different subpopulations of the S_1 state are responsible for the ESA at 800 nm and for the ESA band in the visible. The former, due to a different configuration or a different state energy might be more liable to eject an electron and thus form a cation.

Concluding Remarks

We have used excitation-wavelength-dependent pump−probe, pump−dump−probe, and pump−repump−probe experiments on peridinin in methanol to gain significant insight into its excited-state manifold and dynamics. Dumping the SE of the ICT state with an 800-nm pulse led to a preferential loss of excited-state population, demonstrating that the S_1 and ICT states are discrete. The dynamics observed after the dump illustrate the equilibration of populations between the S_1 and the depleted ICT state taking place within $\sim$5 ps. Furthermore, an unrelaxed ground-state species was identified, implying that the relaxation of peridinin is likely to involve a conformational coordinate. In this picture, this unrelaxed ground state may account for the apparent energy deficit of the ICT state in PCP, where the ICT state transfers energy to Chl-*a* efficiently. Furthermore, we have demonstrated how multipulse experiments can become a valu-

able tool in studying carotenoid cations, which are directly involved in the photoprotective mechanisms of plants.[45]

Our observations illustrate the profound complexity of the excited-state manifold and the excited population dynamics of peridinin. Even though conclusions about peridinin do not necessarily apply to other carotenoids, it is apparent that the overlapping signals and the excitation-wavelength dependence of the excited-state properties require the development and application of new experimental and theoretical approaches before a full characterization is possible.

Acknowledgment. This research was supported by The Netherlands Organization for Scientific Research (NWO) via the Dutch Foundation for Earth and Life Sciences (ALW). D.S.L. is grateful to the Human Frontier Science Program Organization for providing financial support with a long-term fellowship. M.V. received financial support from the Stichting voor Fundamenteel Onderzoek der Materie, Netherlands (FOM).

Supporting Information Available: Figures showing additional PrPP (400-nm excitation, 620-nm repump) and PDP (400-nm pump and 800-nm dump at 3 ps) experiments. This material is available free of charge via the Internet at http://pubs.acs.org.

References and Notes

(1) Falkowski, P. G.; Raven, J. A. *Aquatic photosynthesis*; Blackwell Science, Malden, MA, 1997.

(2) Hiller, R. G. Carotenoids as Components of the Light-harvesting Proteins of Eukaryotic Algae. In *Photochemistry of Carotenoids*; Frank, H. A., Young, A. J., Britton, G., Cogdell, R. J., Eds.; Kluwer Academic Publishers: Dordrecht, The Netherlands, 1999; Vol. 8, p 81.

(3) Mimuro, M.; Nagashima, U.; Takaichi, S.; Nishimura, Y.; Yamazaki, I.; Katoh, T. *Biochim. Biophys. Acta* **1992**, *1098*, 271.

(4) Akimoto, S.; Takaichi, S.; Ogata, T.; Nishimura, Y.; Yamazaki, I.; Mimuro, M. *Chem. Phys. Lett.* **1996**, *260*, 147.

(5) Bautista, J. A.; Connors, R. E.; Raju, B. B.; Hiller, R. G.; Sharples, F. P.; Gosztola, D.; Wasielewski, M. R.; Frank, H. A. *J. Phys. Chem. B* **1999**, *103*, 8751.

(6) Frank, H. A.; Bautista, J. A.; Josue, J.; Pendon, Z.; Hiller, R. G.; Sharples, F. P.; Gosztola, D.; Wasielewski, M. R. *J. Phys. Chem. B* **2000**, *104*, 4569.

(7) Zigmantas, D.; Polívka, T.; Hiller, R. G.; Yartsev, A.; Sundström, V. *J. Phys. Chem. A* **2001**, *105*, 10296.

(8) Zigmantas, D.; Hiller, R. G.; Yartsev, A.; Sundström, V.; Polívka, T. *J. Phys. Chem. B* **2003**, *107*, 5339.

(9) Zimmermann, J.; Linden, P. A.; Vaswani, H. M.; Hiller, R. G.; Fleming, G. R. *J. Phys. Chem. B* **2002**, *106*, 9418.

(10) Shima, S.; Ilagan, R. P.; Gillespie, N.; Sommer, B. J.; Hiller, R. G.; Sharples, F. P.; Frank, H. A.; Birge, R. R. *J. Phys. Chem. A* **2003**, *107*, 8052.

(11) Papagiannakis, E.; Larsen, D. S.; van Stokkum, I. H. M.; Vengris, M.; Hiller, R.; van Grondelle, R. *Biochemistry* **2004**, *43*, 15303

(12) Premvardhan, L. L.; Papagiannakis, E.; Hiller, R.; van Grondelle, R. *J. Phys. Chem. B* **2005**, *109*, 15589−15597.

(13) Bautista, J. A.; Hiller, R. G.; Sharples, F. P.; Gosztola, D.; Wasielewski, M.; Frank, H. A. *J. Phys. Chem. A* **1999**, *103*, 2267.

(14) Krueger, B. P.; Lampoura, S. S.; van Stokkum, I. H. M.; Papagiannakis, E.; Salverda, J. M.; Gradinaru, C. C.; Rutkauskas, D.; Hiller, R. G.; van Grondelle, R. *Biophys. J.* **2001**, *80*, 2843.

(15) Zigmantas, D.; Hiller, R. G.; Sundström, V.; Polívka, T. *Proc. Natl. Acad. Sci. U.S.A.* **2002**, *99*, 16760.

(16) Polívka, T.; Sundström, V. *Chem. Rev.* **2004**, *104*, 2021.

(17) He, Z. F.; Gosztola, D.; Deng, Y.; Gao, G. Q.; Wasielewski, M. R.; Kispert, L. D. *J. Phys. Chem. B* **2000**, *104*, 6668.

(18) Zigmantas, D.; Hiller, R. G.; Sharples, F. P.; Frank, H. A.; Sundstrom, V.; Polívka, T. *Phys. Chem. Chem. Phys.* **2004**, *6*, 3009.

(19) Vaswani, H. M.; Hsu, C. P.; Head-Gordon, M.; Fleming, G. R. *J. Phys. Chem. B* **2003**, *107*, 7940.

(20) Damjanovic, A.; Ritz, T.; Schulten, K. *Biophys. J.* **2000**, *79*, 1695.

(21) Papagiannakis, E.; Kennis, J. T. M.; van Stokkum, I. H. M.; Cogdell, R. J.; van Grondelle, R. *Proc. Natl. Acad. Sci. U.S.A.* **2002**, *99*, 6017.

(22) Walla, P. J.; Linden, P. A.; Ohta, K.; Fleming, G. R. *J. Phys. Chem. A* **2002**, *106*, 1909.

(23) Larsen, D. S.; Vengris, M.; van Stokkum, I. H. M.; van der Horst, M.; de Weerd, F. L.; Hellingwerf, K. J.; van Grondelle, R. *Biophys. J.* **2004**, *86*, 2538.

(24) Larsen, D. S.; Papagiannakis, E.; van Stokkum, I. H. M.; Vengris, M.; Kennis, J. T. M.; van Grondelle, R. *Chem. Phys. Lett.* **2003**, *381*, 733.

(25) Gai, F.; McDonald, J. C.; Anfinrud, P. A. *J. Am. Chem. Soc.* **1997**, *119*, 9, 6201.

(26) Ruhman, S.; Hou, B. X.; Friedman, N.; Ottolenghi, M.; Sheves, M. *J. Am. Chem. Soc.* **2002**, *124*, 8854.

(27) Changenet-Barret, P.; Choma, C.; Gooding, E.; DeGrado, W.; Hochstrasser, R. M. *J. Phys. Chem. B* **2000**, *104*, 9322.

(28) Kovalenko, S. A.; Ruthmann, J.; Ernsting, N. P. *J. Chem. Phys.* **1998**, *109*, 1894.

(29) Logunov, S. L.; Volkov, V. V.; Braun, M.; El-Sayed, M. A. *Proc. Natl. Acad. Sci. U.S.A.* **2001**, *98*, 8475.

(30) Holzwarth, A. R. Data Analysis of Time-Resolved Measurements. In *Biophysical Techniques in Photosynthesis*; Amesz, J., Hoff, A. J., Eds.; Kluwer: Dordrecht, The Netherlands, 1996; p 75.

(31) van Stokkum, I. H. M.; Larsen, D. S.; van Grondelle, R. *Biochim. Biophys. Acta* **2004**, *1657*, 82.

(32) van Stokkum, I. H. M.; Larsen, D. S.; van Grondelle, R. *Biochim. Biophys. Acta* **2004**, *1658*, 262.

(33) Martinson, T. A.; Plumley, F. G. *Anal. Biochem.* **1995**, *228*, 123.

(34) Andersson, P. O.; Gillbro, T. *J. Chem. Phys.* **1995**, *103*, 2509.

(35) de Weerd, F. L.; van Stokkum, I. H. M.; van Grondelle, R. *Chem. Phys. Lett.* **2002**, *354*, 38.

(36) Billsten, H. H.; Zigmantas, D.; Sundström, V.; Polivka, T. *Chem. Phys. Lett.* **2002**, *355*, 465.

(37) Kosumi, D.; Yanagi, K.; Nishio, T.; Hashimoto, H.; Yoshizawa, M. *Chem. Phys. Lett.* **2005**, *408*, 89.

(38) Billsten, H. H.; Pan, J. X.; Sinha, S.; Pascher, T.; Sundstrom, V.; Polivka, T. *J. Phys. Chem. A* **2005**, *109*, 6852.

(39) Horng, M. L.; Gardecki, J. A.; Papazyan, A.; Maroncelli, M. *J. Phys. Chem.* **1995**, *99*, 17311.

(40) Yoshizawa, M.; Aoki, H.; Hashimoto, H. *Phys. Rev. B* **2001**, *63*, 180301.

(41) McCamant, D. W.; Kim, J. E.; Mathies, R. A. *J. Phys. Chem. A* **2002**, *106*, 6030.

(42) Vengris, M.; van Stokkum, I. H. M.; He, X.; Bell, A.; Tonge, P.; van Grondelle, R.; Larsen, D. S. *J. Phys. Chem. B* **2004**, *108*, 4587.

(43) Wohlleben, W.; Buckup, T.; Hashimoto, H.; Cogdell, R. J.; Herek, J. L.; Motzkus, M. *J. Phys. Chem. B* **2004**, *108*, 3320.

(44) Edge, R.; Truscott, T. G. Carotenoid Radicals and the Interaction of Carotenoids with Active Oxygen Species. In *Photochemistry of Carotenoids*; Frank, H. A., Young, A. J., Britton, G., Cogdell, R. J., Eds.; Kluwer Academic Publishers: Dordrecht, The Netherlands, 1999; Vol. 8, p 223.

(45) Holt, N. E.; Zigmantas, D.; Valkunas, L.; Li, X.-P.; Niyogi, K. K.; Fleming, G. R. *Science* **2005**, *307*, 433.